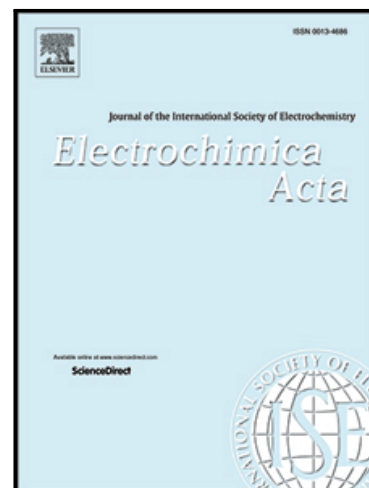


Operando Characterization of Active Surface Area and Passivation Effects on Sulfur-Carbon Composites for Lithium-Sulfur Batteries

He Li , John Lampkin , Yu-Chuan Chien , Liam Furness ,  
Daniel Brandell , Matthew J. Lacey , Nuria Garcia-Araez

PII: S0013-4686(21)01856-9  
DOI: <https://doi.org/10.1016/j.electacta.2021.139572>  
Reference: EA 139572



To appear in: *Electrochimica Acta*

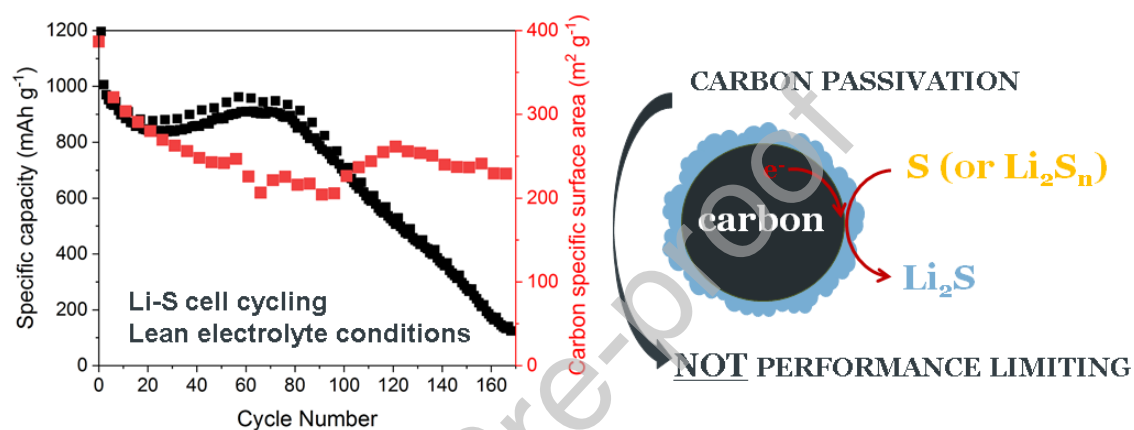
Received date: 9 September 2021  
Revised date: 30 October 2021  
Accepted date: 9 November 2021

Please cite this article as: He Li , John Lampkin , Yu-Chuan Chien , Liam Furness , Daniel Brandell , Matthew J. Lacey , Nuria Garcia-Araez , Operando Characterization of Active Surface Area and Passivation Effects on Sulfur-Carbon Composites for Lithium-Sulfur Batteries, *Electrochimica Acta* (2021), doi: <https://doi.org/10.1016/j.electacta.2021.139572>

This is a PDF file of an article that has undergone enhancements after acceptance, such as the addition of a cover page and metadata, and formatting for readability, but it is not yet the definitive version of record. This version will undergo additional copyediting, typesetting and review before it is published in its final form, but we are providing this version to give early visibility of the article. Please note that, during the production process, errors may be discovered which could affect the content, and all legal disclaimers that apply to the journal pertain.

## Highlights

- First quantification of the passivation of the carbon matrix in Li-S batteries
- Electrochemically active specific surface area of carbon quantified by impedance
- Method of analysis validated with model carbon and carbon-sulfur composite electrodes



# Operando Characterization of Active Surface Area and Passivation Effects on Sulfur-Carbon Composites for Lithium-Sulfur Batteries

He Li<sup>†,1,2</sup>, John Lampkin<sup>†,1</sup>, Yu-Chuan Chien<sup>†,3</sup>, Liam Furness<sup>1,4</sup>, Daniel Brandell<sup>3</sup>, Matthew J. Lacey<sup>3,5</sup>, and Nuria Garcia-Araez<sup>\*1,4</sup>

<sup>†</sup>These authors contributed equally to this work

<sup>1</sup> School of Chemistry, University of Southampton, Southampton, SO17 1BJ, United Kingdom

<sup>2</sup> College of Environmental Science and Engineering, North China Electric Power University, Beijing 102206, China

<sup>3</sup> Department of Chemistry, Ångström Laboratory, Uppsala University, Box 538, Lägerhyddsvägen 1, 751 21 Uppsala, Sweden

<sup>4</sup> The Faraday Institution, Harwell Campus, Didcot, OX11 0RA, United Kingdom

<sup>5</sup> Scania CV AB, 151 87 Södertälje, Sweden

\* Corresponding author: n.garcia-araez@soton.ac.uk (Nuria Garcia-Araez)

## Abstract

Sulfur electrodes for lithium-sulfur batteries necessarily contain a conductive additive, typically carbon, to enable the electrochemical reactions, since sulfur and the discharge product, Li<sub>2</sub>S, are insulators. Consequently, the full passivation of carbon, by deposition of sulfur and/or Li<sub>2</sub>S, would necessarily produce the death of the battery. However, here we demonstrate that for high-performance lithium-sulfur batteries operated under lean electrolyte conditions (electrolyte to sulfur ratio of 6  $\mu\text{L mg}_\text{S}^{-1}$  in Li-S coin cells), the extent of passivation of carbon is not severe enough to limit performance. This is shown by performing impedance measurements of fully charged lithium-sulfur batteries, from which we demonstrate that we can evaluate the specific surface area of carbon, and we find that the capacity fade with cycling is not due to a decrease in the electrochemically active surface area of carbon. These results show that introducing a higher surface area carbon in the sulfur electrode formulation is not needed to prevent passivation, and that the focus of lithium-sulfur development should be directed towards other issues, such as mitigating undesirable reactions at the lithium electrode and achieving robust sulfur electrode structures enabling fast transport of electrolyte species and, thus, more homogeneous reactions.

Keywords: Lithium-sulfur batteries; electrochemical impedance spectroscopy; passivation; mass transport; capacity fade; cathode.

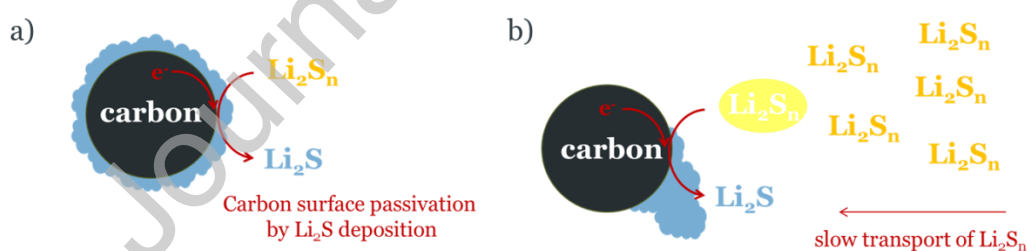
## 1. Introduction

The lithium-sulfur (Li-S) battery currently stands as one of the most promising beyond Li-ion battery candidates, with very high prospective values of gravimetric energy density, very low projected cost due to the use of sulfur, and absence of scarce elements such as cobalt or nickel [1-5]. Impressive technology advances have been achieved in the last years, with innovations

in materials, techniques and mechanistic understanding of the reactions, which have brought the Li-S batteries closer to large-scale commercialisation. However, significant performance improvements need to be achieved in order to expand the commercial applications of Li-S batteries; specifically improvements in cycle life and/or power are critical [4], but progress is hampered by the lack of understanding of the key processes limiting such important performance metrics.

Figure 1 illustrates the two main fundamental factors, related to the sulfur electrode, that have been proposed to limit the operation of Li-S batteries: a) surface passivation phenomena, and b) mass transport limitations. The decisive effect of mass transport effects in limiting the operation of Li-S batteries has been recently demonstrated by combining theoretical and experimental observations [6, 7]. As the Li-S battery discharges, solid sulfur is converted into soluble polysulfides and then finally into  $\text{Li}_2\text{S}$ , but when the rate of transport of polysulfides to the sulfur electrode surface is not fast enough, to hold the required current, the end of discharge is reached. More recently, operando X-ray diffraction measurements of Li-S batteries suggested that the slow transport of polysulfides at the end of discharge is due to the blocking of the pores of the sulfur electrode by  $\text{Li}_2\text{S}$  deposition [8]. In addition, X-ray tomography characterisation of Li-S batteries reveal drastic morphological changes undergone by the sulfur electrode during cycling, which could cause capacity fade with cycling [9-12].

On the other hand, sulfur and  $\text{Li}_2\text{S}$  are both insulator materials and therefore, if the carbon conductive additive became fully covered by sulfur and/or  $\text{Li}_2\text{S}$ , then its electrochemical activity would be suppressed (an effect known as passivation), and consequently it would not be possible to maintain the electrochemical reactions, since the other components in the sulfur electrode formulation (sulfur,  $\text{Li}_2\text{S}$ , binder) are insulators. Clearly, the deposition of sulfur or  $\text{Li}_2\text{S}$  on the carbon matrix in sulfur electrodes can be a very important factor affecting the performance of Li-S batteries, as pointed out previously [13-21]. However, due to the lack of an experimental technique able to probe the extent of passivation, the effect of passivation phenomena in practical Li-S batteries has remained unresolved until now.



**Figure 1.** Schematic illustration of the two main effects, related to the sulfur electrode, that have been suggested to limit Li-S battery performance: a) complete passivation of the carbon conductive additive, and b) slow rate of mass transport of polysulfides to the electrochemically active carbon particles.  $\text{Li}_2\text{S}$  deposits are shown in blue, the black particle is carbon and lithium polysulfides ( $\text{Li}_2\text{S}_n$ ) are shown in yellow. In a) the full coverage of the carbon surface by  $\text{Li}_2\text{S}$  deposits prevents any further electrochemical reactions. In b)  $\text{Li}_2\text{S}_n$  close to the carbon particle is shown in white to illustrate the depletion of polysulfides, which thus impedes further polysulfide reduction.

Here we report the development of a new approach, using impedance spectroscopy, that is able to quantify, in-situ, the electrochemically active surface area of the carbon matrix in sulfur electrodes for Li-S batteries. This new approach enables the quantification of the degradation of carbon, as a function of the battery cycle number, and thus provides a quantitative measure of detrimental phenomena such as the disconnection of the carbon particles from the current

collector or suppression of their electrochemical activity due to passivation by  $\text{Li}_2\text{S}$  or sulfur deposition. However, we find experimentally that the decrease in capacity with cycling is not correlated with a decrease in the electrochemically active surface area of carbon, and thus, we conclude that electrode passivation is not a factor that limits the operation of Li-S batteries.

## 2. Theory

### 2.1. Evaluation of the specific surface area of carbon and carbon-sulfur composite electrodes in symmetrical cell experiments

The impedance of symmetrical cells containing two porous carbon electrodes (or two carbon-sulfur composite electrodes), impregnated with the liquid electrolyte and separated by a separator, also impregnated by the liquid electrolyte, can be described as:

$$Z_{\text{symmetrical cell}} = 2Z_{\text{electrode}} + R_{\text{electrolyte}} \quad (1)$$

where  $R_{\text{electrolyte}}$  is the resistance of the electrolyte-impregnated separator and  $Z_{\text{electrode}}$  is the impedance of the electrolyte-impregnated porous carbon (or carbon-sulfur) electrode. The factor of 2 multiplying  $Z_{\text{electrode}}$  in equation (1) is because the cell contains two identical electrodes.

The impedance of the porous carbon or carbon-sulfur electrode can be modelled with de Levie Pore finite length element ( $L_s$ ) in ZView [22, 23]:

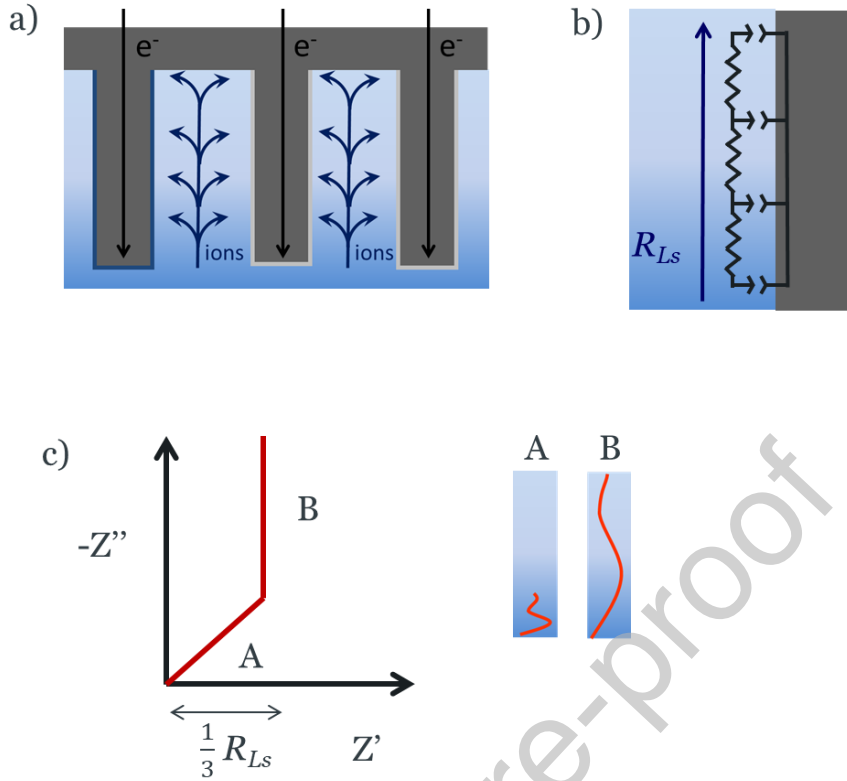
$$Z_{L_s} = \frac{R_{L_s}}{\Lambda^{1/2}} \coth[\Lambda^{1/2}] \quad \text{where } \Lambda = \frac{1}{A_{L_s}} + B_{L_s} (i\omega)^{\phi_{L_s}} \quad (2)$$

where  $i$  is the imaginary number,  $\omega$  is the angular frequency (in rad/s),  $\coth$  is the hyperbolic cotangent,  $R_{L_s}$  is the electrolyte resistances inside the pores,  $B_{L_s}$  is proportional to the electrode effective capacitance,  $A_{L_s}$  is proportional to the charge-transfer resistance and  $\phi_{L_s}$  is the constant phase exponent (for a perfect capacitor,  $\phi_{L_s}$  is equal to 1). See the supporting information for details about the meaning of the parameters.

Since charge-transfer reactions of sulfur reduction to polysulfides are absent under our experimental conditions, the fitting of the impedance data is done by fixing the  $A_{L_s}$  parameter, proportional to the charge transfer resistance, to a very large number (e.g.  $10^{20}$ ). This approach is mathematically identical to using an open Warburg element in ZView,  $W_o$ , as shown in the supporting information, and indeed, in previous work we employed the open Warburg element to describe the impedance response of porous electrodes [24, 25].

De Levie Pore finite length element is used here to describe a porous electrode in which ions are transported within the electrolyte filling the electrode's pores while the electrode-electrolyte interphase undergoes double-layer charging (Figure 2a). As mentioned above, the absence of charge-transfer reactions is incorporated by fixing the  $A_{L_s}$  parameter to a very large number. This element represents a transmission line of electrolyte resistors and double-layer capacitors (Figure 2b) and it produces a characteristic impedance response (Figure 2c) that, in the Nyquist plot, consists of a 45-degree line at high frequencies (region A, where the rate of ion transport is not fast enough to fully penetrate the pores at the high measurement

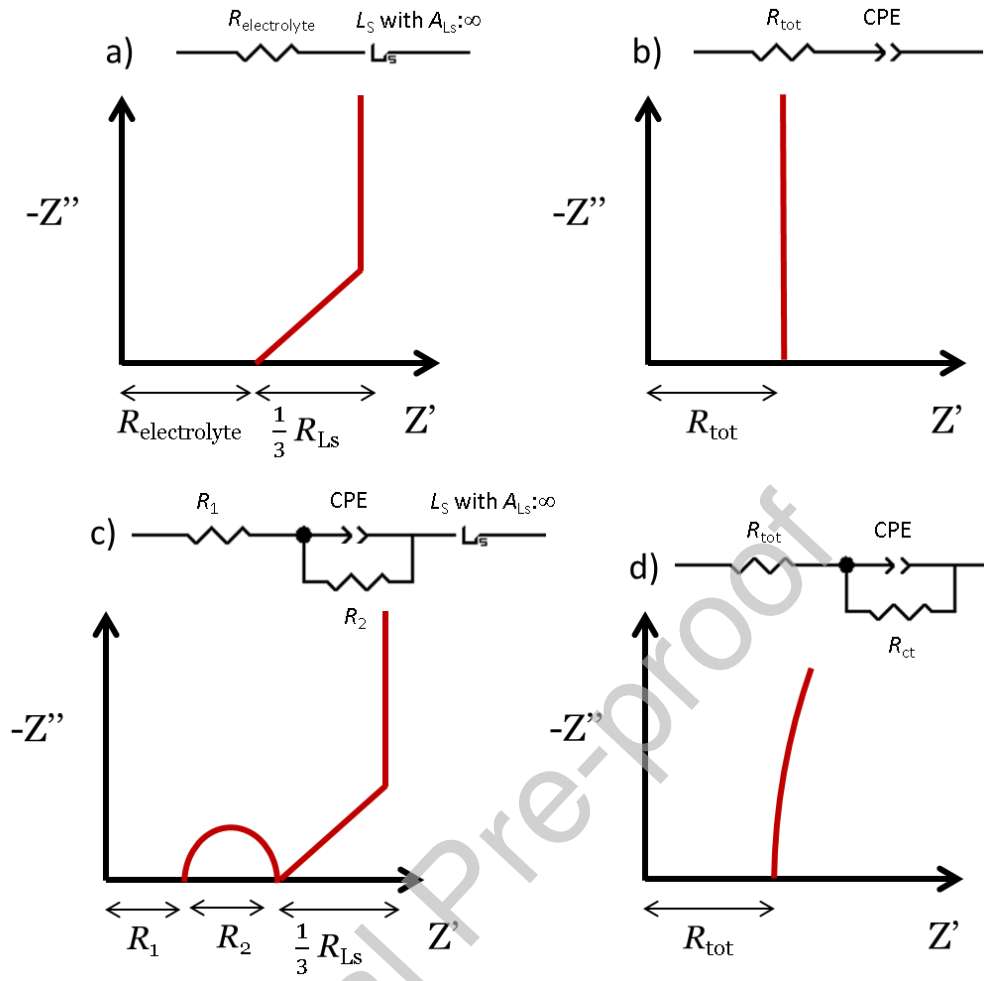
frequencies) followed by a vertical line at low frequencies (region B, where ion transport is given enough time, at the lower measurement frequencies, to fully penetrate the pores).



**Figure 2.** Physical meaning of the de Levie Pore finite length element used here to represent a porous electrode with only double-layer charging (no charge-transfer) reactions. a) Schematic illustration of the transport of ions within the electrolyte-filled pores and of electrons within the electrode, as required to hold the double-layer charging reactions at the electrode-electrolyte interphase. b) Schematic illustration of the transmission line of resistors (due to ion transport within the pores) and capacitors (due to charging of the electrode-electrolyte interface). c) Illustration of the impedance response in the Nyquist plot, where in region A ion transport is slow compared to the impedance frequency and thus the transport of ions does not penetrate the pores fully, while in region B ion transport is fast compared to the impedance frequency and thus the transport of ions fully penetrates the pores. For simplicity, the impedance plot illustrates the ideal behaviour with unity value of the exponent of de Levie element.

Therefore, the impedance of symmetrical cells with carbon (or carbon-sulfur) electrodes can be fitted to an equivalent circuit with de Levie Pore finite length element connected to a resistor in series, as shown in figure 3a. (Note that only one de Levie Pore finite length element is used to represent the two electrodes in the cell; the impedance of one electrode would be half of the impedance of de Levie Pore finite length element). Similar approaches have been taken before to study Li-S [24, 26] and Li-ion batteries [27-32]. The results of the fit give the values of the resistance of the electrolyte,  $R_{electrolyte}$ , and the characteristic properties of de Levie Pore finite length element ( $R_{Ls}$ ,  $B_{Ls}$  and  $\phi_{Ls}$ ;  $A_{Ls}$  is fixed here to  $10^{20}$ ). With the results of the fitting, the effective capacitance parameter of the cell,  $Q_{Ls}$ , can be obtained from:

$$Q_{Ls} = \frac{B_{Ls}}{R_{Ls}} \quad (3)$$



**Figure 3.** Equivalent circuits used to fit impedance data, and their corresponding impedance response. a) Resistor coupled, in series, to a de Levie Pore finite length element with infinite charge transfer resistance. b) Resistor coupled, in series, to a constant phase element (CPE). c) Resistor coupled, in series, to a combination of a CPE and a resistor in parallel, and then coupled, in series, to a de Levie Pore finite length element with infinite charge transfer resistance. d) Resistor coupled, in series, to a combination of a CPE and a resistor in parallel. For simplicity, the impedance plots illustrate the ideal behaviour with unity values of the exponent of the CPE and de Levie elements.

The effective capacitance parameter,  $Q_{LS}$ , is not a pure double-layer capacitance, and it has units of  $F s^{\phi_{LS}-1}$ . Considering that the deviations from the ideal behaviour are due to surface inhomogeneity, the following equation can be used to calculate the average double-layer capacitance of the cell,  $\bar{C}_{dl,cell}$  [33-36]:

$$\bar{C}_{dl,cell} = (Q_{LS})^{\frac{1}{\phi_{LS}}} (R_{tot})^{\frac{1-\phi_{LS}}{\phi_{LS}}} \quad (4)$$

where  $R_{tot}$  is the total resistance:

$$R_{tot} = R_{electrolyte} + \frac{R_{LS}}{3} \quad (5)$$

where  $R_{electrolyte}$  is the resistance of the electrolyte-impregnated separator and  $R_{LS}$  is the resistance of the electrolyte-impregnated pores of the porous electrodes (both  $R_{electrolyte}$  and  $R_{LS}$  are obtained from the fitting).

Then, the double-layer capacitance of one electrode,  $\bar{C}_{dl,electrode}$ , is obtained by multiplying  $\bar{C}_{dl,cell}$  by a factor of 2, to take into account that the cell contains two electrodes connected in series:

$$\bar{C}_{dl,electrode} = 2\bar{C}_{dl,cell} \quad (6)$$

From the value of the capacitance of one electrode,  $\bar{C}_{dl,electrode}$ , it is possible to estimate the total electrochemically active surface area, SA, by taking into account that a typical value of the area-normalized double-layer capacitance of carbon materials is  $C_{sp,dl} = 10 \mu F cm^{-2}$  [37].

$$SA = \frac{\bar{C}_{dl,electrode}}{C_{sp,dl}} \quad (7)$$

The total effective surface area, SA, is associated with the surface area of carbon particles in contact with the electrolyte (since other materials in the electrode, such as binder and sulfur, are electrochemically inactive). Therefore, for the evaluation of the effective specific surface area, SSA, the values of surface area, SA, as described in equation 7 are divided by the mass of carbon in the electrode,  $m_C$ .

$$SSA = \frac{SA}{m_C} \quad (8)$$

The analysis described above allows fitting the impedance response of porous carbon or carbon-sulfur electrodes in the whole frequency range. Alternatively, it is possible to restrict the fit to the low-frequency range, in which ion transport is fast enough to fully penetrate all the pores of the porous electrodes and therefore the electrode response is that of a blocking electrode and can be represented by a constant phase element (CPE):

$$Z_{CPE} = \frac{1}{Q_{CPE}(i\omega)^{P_{CPE}}} \quad (9)$$

where  $Q_{CPE}$  is the characteristic capacitance parameter associated to the CPE element and has units of  $F s^{P_{CPE}-1}$ , and  $P_{CPE}$  is the exponent of the CPE element (for an ideal capacitor,  $P_{CPE}=1$ ). Note that the capacitance parameter  $Q_{CPE}$  is often denoted by the symbol  $T$  (in ZView, for example), but we have here retained the symbol  $Q$  to distinguish it from a time constant parameter.



By fitting the impedance data of the symmetrical cell in the low frequency range, using a resistor coupled to a CPE in series (see Figure 3b), the total double-layer capacitance of the cell is obtained from [33-36]:

$$\bar{C}_{dl,cell} = (Q_{CPE})^{\frac{1}{P_{CPE}}} (R_{tot})^{\frac{1-P_{CPE}}{P_{CPE}}} \quad (10)$$

where  $R_{tot}$  is the value of resistance (obtained from the fitting).

It will be shown below that the methods of analysis using the whole frequency range (equivalent circuit in Figure 3a) and the lower-frequency range (equivalent circuit in Figure 3b) produce the same values (within 8%) of the surface area, SA, and specific surface area, SSA.

In some cases, the impedance results show a semicircle at high frequencies, which can be attributed to an electronic contact resistance between the current collector and the electrode coating [24, 28, 38] (and such contact resistance can be larger on the electrode edges, depending on the electrode cutting technique [39]). In these cases, the fit of the impedance data at all frequencies is done with the equivalent circuit in Figure 3c, and the values of SA and SSA, are obtained using equations (3-8) with  $R_{electrolyte} = R_1 + R_2$ . Again, as will be shown below, the surface area results are consistent with the values obtained by using the equivalent circuits in Figure 3a,b.

Finally, in some cases, the impedance results at low frequencies show a curvature, suggesting the presence of a very sluggish charge-transfer reaction. In these cases, the fitting is done with an equivalent circuit consisting of a resistor coupled in series to the combination of a CPE and a resistor in parallel (equivalent circuit in Figure 3d). Then, the total double layer capacitance of the cell is obtained from [33-36]:

$$\bar{C}_{dl,cell} = (Q_{CPE})^{\frac{1}{P_{CPE}}} \left( \frac{R_{tot} R_{ct}}{R_{tot} + R_{ct}} \right)^{\frac{1-P_{CPE}}{P_{CPE}}} \quad (11)$$

## 2.2 Evaluation of the specific surface area of carbon-sulfur composite electrodes in Li-S cell experiments

The impedance of Li-S cells with liquid electrolyte and separator can be described as:

$$Z_{Li-S} = Z_{sulfur} + R_{electrolyte} + Z_{Li} \quad (12)$$

where  $R_{electrolyte}$  is the resistance of the electrolyte-impregnated separator,  $Z_{sulfur}$  is the impedance of the electrolyte-impregnated porous carbon-sulfur composite electrode and  $Z_{Li}$  is the impedance of the lithium electrode.

While the analysis of impedance of Li-S cells is complicated [40-54], we here simplify the analysis by studying the Li-S cells in the fully charged state. As a result of the use of optimised electrode and electrolyte formulations, the Li-S cells in this work show negligible overcharge problems and absence of polysulfide shuttling current in the fully charge state, as expected for the full conversion of polysulfides into sulfur. Therefore, under our experimental conditions, the concentration of polysulfides in the fully charged Li-S cells is minimal, and thus the

polysulfide charge-transfer reactions have very slow kinetics. In essence, the sulfur electrode behaves as a porous double-layer capacitor, as in the experiments with sulfur electrodes in symmetrical cells, so it can be represented by a de Levi Pore finite length element (Ls) or, by restricting the fit to low frequencies, by a constant phase element (CPE). On the other hand, the impedance of the lithium electrode is also complicated, but by restricting the fit to low frequencies, it can be represented by a simple resistor. Therefore, the analysis of the impedance of fully charged Li-S cells is done with an equivalent circuit consisting of a resistor coupled to a CPE in series (equivalent circuit in Figure 3b). With the results of the fitting, total double-layer capacitance of the sulfur electrode is obtained from [33-36]:

$$\bar{C}_{dl, electrode} = (Q_{CPE})^{\frac{1}{P_{CPE}}} (R_{tot})^{\frac{1-P_{CPE}}{P_{CPE}}} \quad (13)$$

In some cases, the impedance of Li-S cells at low frequencies is affected by a slow charge-transfer reaction. In these cases, the fitting is done with an equivalent circuit consisting of a resistor coupled in series to the combination of a CPE and a resistor in parallel (equivalent circuit in Figure 3d). Then, the double-layer capacitance of the sulfur electrode is obtained from [33-36]:

$$\bar{C}_{dl, electrode} = (Q_{CPE})^{\frac{1}{P_{CPE}}} \left( \frac{R_{tot} R_{ct}}{R_{tot} + R_{ct}} \right)^{\frac{1-P_{CPE}}{P_{CPE}}} \quad (14)$$

### 3. Experimental section

#### 3.1 Materials

Sulfur powder (S, Sigma-Aldrich), Ketjenblack (KB, EC-600JD, AkzoNobel), Super C65 (Imerys), carbon nanofibers (CNF, 20-200 nm × 100 μm, Sigma-Aldrich), carbon nanotubes (CNT, 6-13 nm × 2.5-20 μm, Sigma-Aldrich), poly(ethylene oxide) (PEO,  $M_w \sim 4,000,000$ , Sigma-Aldrich) and polyvinylpyrrolidone (PVP,  $M_w \sim 360,000$ , Sigma-Aldrich) were used as received. Lithium metal foil (Li, Cyprus Foote Mineral, 125 μm thick) was used as received but stored under Argon atmosphere to avoid oxidation. Lithium bis(trifluoromethanesulfonyl)imide (LiTFSI, Sigma-Aldrich) and lithium nitrate ( $LiNO_3$ , Sigma-Aldrich) were dried at 120 °C under vacuum overnight. 1,3-Dioxolane (DOL, Sigma-Aldrich) and 1,2-dimethoxyethane (DME, Sigma-Aldrich) were dried with 3 Å molecular sieves overnight.

#### 3.2 Electrode preparation

CNT electrodes were made of 88% CNT, 8% PEO and 4% PVP (percentages by weight). CNT was ground in an agate mortar for 20 minutes and was then added into a pre-dissolved binder solution, made by dissolving PEO and PVP in solvent mixture with acetonitrile (HiPerSolv, ACS) and ethanol (Fisher, ≥99.8% analytical grade) in a 2:1 volume ratio. The resulting ink was mixed with a magnetic stirring bar for no less than 2 h, and then the ink was coated onto a pre-cut and cleaned Mo foil (25 μm thickness, ≥99.9 % trace metals basis, Sigma-Aldrich) or onto Cu foil (50 μm thickness, 99.95+% purity, Goodfellow Cambridge Ltd) or Al foil (35 μm thickness, 99.2% purity, Advent Research Materials) with a doctor blade coater (TQC Sheen). After the acetonitrile and ethanol had evaporated, the electrode sheet was punched into 11 mm discs with a hand-held punch (Hohsen Corp.) and dried under vacuum in a Büchi tube at 60 °C for no less than 24 h, before transferring into an Ar filled glovebox ( $H_2O$  and  $O_2 \leq 5$  ppm).

S/CNT electrodes were made of 58.8% S, 29.4% CNT, 7.9% PEO and 3.9% PVP (percentages by weight). S and CNT were mixed by grinding in an agate mortar for 10 minutes, then transferred

into a PTFE autoclave, sealed tightly, and heated at 155 °C for 6.5 h to impregnate CNT with S. After cooling down, the mixture of S and CNT was ground again with an agate mortar for 20 minutes before adding it into PEO and PVP binder solution (same procedure as CNT only electrodes). After mixing with a magnetic stirring bar for no less than 2 h, the ink was coated onto a pre-cut and cleaned Mo foil or Al foil. After the acetonitrile and ethanol had evaporated, the electrode sheet was punched into 11 mm discs with a hand-held punch (Hohsen Corp.) and dried under vacuum in a Büchi tube at room temperature (20-25 °C) for no less than 2 days, before transferring into an Ar filled glovebox ( $\text{H}_2\text{O}$  and  $\text{O}_2 \leq 5$  ppm).

S/C electrodes developed to produce high performance Li-S batteries, here called 'optimised S/C electrodes', were made of 65% S, 21% KB, 3.5% C65, 3.5% CNF, 5.6% PEO and 1.4% PVP (percentage by weight). The procedure of making the optimised S/C electrodes can be found in previously published papers [8, 55-57].

### 3.3 Cell construction and characterisation

The impedance measurements of symmetrical cells were done with Swagelok-type cells, as described previously [24]. All cell components were cleaned using ethanol and dried in a 70 °C fan-assisted oven overnight before transferring into a glovebox. Copper rods and caps were polished by SiC sandpaper (P1200, 3M) and alumina polishing powder (from 25  $\mu\text{m}$  to 3  $\mu\text{m}$ , 0.3  $\mu\text{m}$  and 0.05  $\mu\text{m}$ ) until the copper surface shined like a mirror. Cells were half-assembled outside glovebox by fixing one copper rod into the stainless-steel cell body with perfluoroalkoxy alkane (PFA) ferrules, where Mylar film was used to line the inside of the cell body to prevent contact between the electrodes and the cell body. The CNT or CNT/S electrodes (described in 3.2, 11 mm diameter) were weighed inside glovebox with a 4-digit balance (OHAUS Adventurer<sup>TM</sup>, AR0640), and the cells were assembled with two nearly identical electrodes (difference in weight < 0.2 mg). Two Whatman GF/F glass microfiber filters (12 mm diameter) were used as separators and 120  $\mu\text{L}$  of electrolyte (1 M LiTFSI in DOL:DME, 1:1 v/v, with 0.25 M  $\text{LiNO}_3$  as additive) were added to the cell. After assembly inside the glovebox, the cells were placed in a Memmert climatic chamber set to 25 °C for the electrochemical characterization. The cells were allowed to equilibrate for 6 h and then the PEIS measurements were performed with a voltage amplitude of 10 mV and a frequency range of 200 kHz - 10 mHz using a VMP3 potentiostat (BioLogic).

Li-S cells were prepared in CR2025 coin cells. The cells comprised an optimised S/C electrode (described in 3.2, 13 mm diameter), a porous polypropylene separator (Celgard<sup>®</sup> 2400, 17 mm diameter) and Li disc counter electrode (Cyprus Foote Mineral, 125  $\mu\text{m}$  thick, 15 mm diameter). The electrolyte was the same as in symmetrical cell studies (1 M LiTFSI in DOL:DME, 1:1 v/v, with 0.25 M  $\text{LiNO}_3$  as additive) and the electrolyte to sulfur ratio was 6  $\mu\text{L mg}_\text{S}^{-1}$ , which corresponds to a molar ratio of  $\text{Li}^+$  to S of 0.24. Cells were allowed to equilibrate at the open circuit voltage (OCV) for 6 h (in which the OCV varied slightly from ca. 3.0 to 2.9 V) and, then, PEIS measurements of the 'pristine cell' were performed using a MPG 2 potentiostat (BioLogic), with the same impedance settings mentioned above. Subsequently, the Li-S cells were discharged at C/50 ( $C = 1672 \text{ mAh g}_\text{S}^{-1}$ ) to 1.9 V and charged at C/25 to 2.8 V in the first cycle, after which a PEIS measurement was conducted. From the second cycle on, the cells were cycled with galvanostatic cycling with potential limitation (GCPL), employing a lower and upper voltage limit of 1.8 V and 2.6 V, respectively, at C/10. In addition, every 5 cycles, the Li-S cells were cycled to an upper voltage limit of 2.8 V, and after a voltage hold of 1 h, PEIS measurements of the cycled cells were conducted.

All the impedance measurements have been normalised by the carbon or sulfur electrode area (0.95  $\text{cm}^2$  for the measurements in symmetrical cells and 1.33  $\text{cm}^2$  for the Li-S cells).

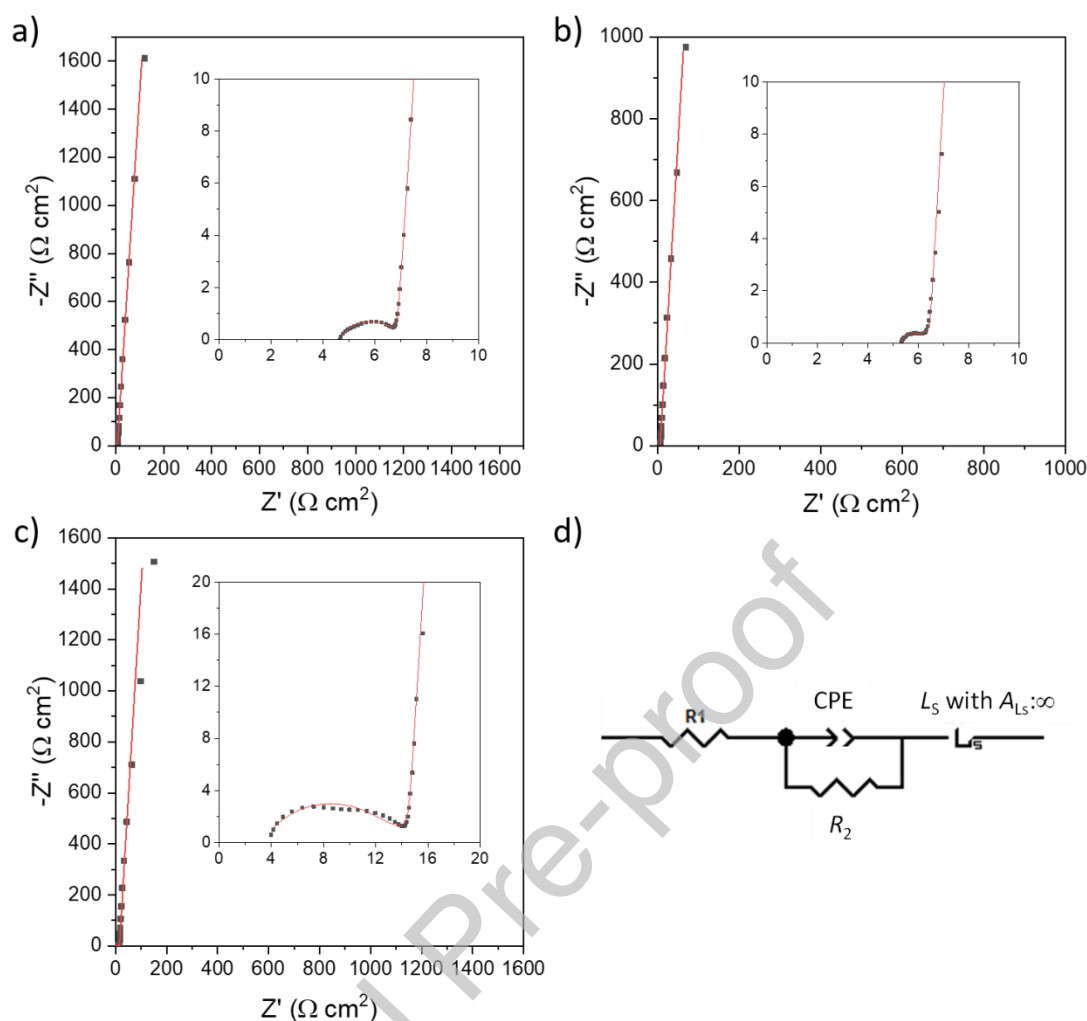
N<sub>2</sub> adsorption measurements were performed on a Micromeritics Tristar II surface area analyser for the evaluation of the Brunauer-Emmet-Teller (BET) surface area. Prior to the measurements, the materials were dried at 120 °C (or room temperature for materials containing sulfur) in a pre-dried sample tube, using a Gas Adsorption Sample Preparation Device (micromeritics, VacPrep 061 Sample Degas System), until the mass remained constant as measured in 30-minute intervals.

## 4. Results and discussion

### 4.1. Validation of the evaluation of specific surface areas by impedance measurements

The reliability of the use of impedance measurements for the evaluation of the specific surface areas of carbon and carbon-sulfur composite electrodes was first evaluated using a simple formulation of the electrodes, made with only one type of carbon (in this case, multi-walled carbon nanotubes, CNT), mixed with a binder (in this case, PEO and PVP). CNT have low surface roughness, which improves the reliability of the surface area evaluation, and PEO and PVP have been used before to produce high-performance electrodes for Li-S batteries [8, 55-57].

The impedance results of the CNT electrodes in symmetrical cells (containing two nearly-identical CNT electrodes, separated by a separator with liquid electrolyte) are shown in figure 4. The electrodes were coated on three different substrates: copper (Figure 4a), molybdenum (Figure 4b) and aluminium (Figure 4c), and it is seen that the high frequency semicircle is small for the electrodes deposited on copper and molybdenum, but it is much larger for electrodes coated on aluminium. This high frequency semicircle has been ascribed to a contact resistance between the electrode coating and the substrate [24, 28, 58], and hence it is understandable that the magnitude of the semicircle (that is, the contact resistance) increases with substrates such as aluminium that contain a poorly conductive oxide layer of significant thickness. Indeed, such high frequency semicircle, due to a contact resistance, is completely absent when the measurements are done with self-standing carbon electrodes (supporting information Figure S1).

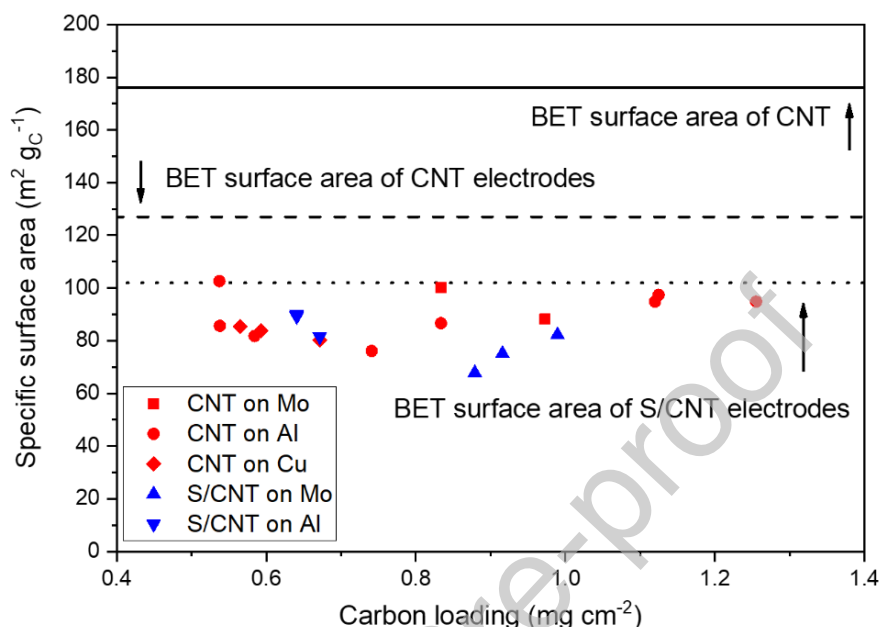


**Figure 4.** Impedance response of symmetrical cells with CNT electrodes coated on a) Cu foil, b) Mo foil and c) Al foil (with enlarged figures inset). The CNT electrodes contain CNT and binder (PEO+PVP) in a mass ratio of 88:12. The red lines show the fit to d) the equivalent circuit. Impedance values are normalised by the electrode geometrical area.

Table 1 summarises the results of the specific surface area evaluation using different equivalent circuit models for the CNT electrodes deposited on the three different substrates (for details about the calculations, see the theory section). In all cases, the specific surface area values are normalised by the mass of carbon, since the binder is electrochemically inactive and will thus not contribute to the impedance response. Table 1 shows that the different fitting methods provide values of the specific surface area that are fully consistent (with less than 10% of variation). The differences in surface area of electrodes coated on different substrate materials are within the cell-to-cell variations of these measurements. Figure 5 shows repeats of these experiments, as a function of the carbon loading, and the differences between the specific surface area values can be attributed to the intrinsic cell-to-cell variability (originating from the manual method of electrode preparation and cell assembly, and the uncertainty in the evaluation of the carbon loading).

The validity of the method of evaluation of surface areas was then corroborated with electrodes made with another type of carbon. Table S1 in the supporting information shows

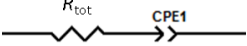
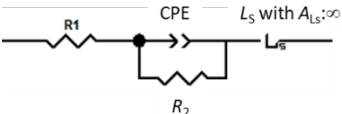

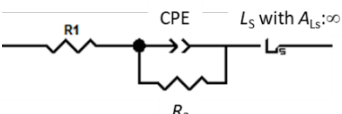
the results of the specific surface area evaluation for self-standing carbon electrodes made by mixing acetylene black carbon and PTFE binder. Again, consistent values of surface areas are observed for the different fitting procedures, demonstrating the validity of the analysis. In addition, Table S1 also shows the evaluation of the surface area of the same type of carbon electrodes, but using impedance measurements of cells with a Li counter electrode. Again, the results are in very good agreement.



**Figure 5.** Results of the specific surface area (SSA) of carbon in CNT and S/CNT electrodes, coated on different substrates, as indicated. The SSA values have been obtained by fitting the impedance data to the equivalent circuit in Figure 3b, but consistent values are obtained with other fitting methods (see table 1). The results of the BET specific surface areas are also shown to facilitate comparison. The specific surface area values are normalised by the mass of carbon, and the carbon loading values are normalised by the geometrical area of the electrode.

**Table 1.** Comparison of the results of the specific surface area evaluation for CNT electrodes from the impedance data in Figure 4. The specific surface area values are normalised by the mass of carbon, and the results of the impedance fitting are normalised by the geometrical area of the electrode.

Electrode substrate	Equivalent circuit	Frequency range for fitting	Results from fitting	Specific surface area / m <sup>2</sup> g <sup>-1</sup>
Cu		176 Hz – 10 mHz	$R_{tot} = 6.83 \, \Omega \, \text{cm}^2$ , $Q_{CPE} = 0.00286 \, \mu\text{F} \, \text{cm}^{-2} \, \text{s}^{P_{CPE}-1}$ , $P_{CPE} = 0.959$ .	85
Cu		200 kHz – 10 mHz	$R_1 = 4.63 \, \Omega \, \text{cm}^2$ , $R_2 = 2.06 \, \Omega \, \text{cm}^2$ , $Q_{CPE} = 3.66 \times 10^{-4} \, \mu\text{F} \, \text{cm}^{-2} \, \text{s}^{P_{CPE}-1}$ , $P_{CPE} = 0.690$ , $R_{Ls} = 0.580 \, \Omega \, \text{cm}^2$ , $B_{Ls} = 1.65 \times 10^{-3} \, \text{s}^{\phi_{Ls}}$ , $\phi_{Ls} = 0.960$ .	85

Mo		119 Hz – 10 mHz	$R_{tot} = 6.40 \, \Omega \, \text{cm}^2$ , $Q_{CPE} = 0.00480 \, \mu\text{F} \, \text{cm}^{-2} \, \text{s}^{P_{CPE}-1}$ , $P_{CPE} = 0.962$ .	100
Mo		200 kHz – 10 mHz	$R_1 = 5.31 \, \Omega \, \text{cm}^2$ , $R_2 = 0.502 \, \Omega \, \text{cm}^2$ , $Q_{CPE} = 9.93 \times 10^{-5} \, \mu\text{F} \, \text{cm}^{-2} \, \text{s}^{P_{CPE}-1}$ , $P_{CPE} = 1.01$ , $R_{Ls} = 1.86 \, \Omega \, \text{cm}^2$ , $B_{Ls} = 8.90 \times 10^{-3} \, \text{s}^{\phi_{Ls}}$ , $\phi_{Ls} = 0.963$	100
Al		2.3 Hz – 10 mHz	$R_{tot} = 14.4 \, \Omega \, \text{cm}^2$ , $Q_{CPE} = 0.00312 \, \mu\text{F} \, \text{cm}^{-2} \, \text{s}^{P_{CPE}-1}$ , $P_{CPE} = 0.962$ .	103
Al		200 kHz – 10 mHz	$R_1 = 3.30 \, \Omega \, \text{cm}^2$ , $R_2 = 9.90 \, \Omega \, \text{cm}^2$ , $Q_{CPE} = 6.48 \times 10^{-5} \, \mu\text{F} \, \text{cm}^{-2} \, \text{s}^{P_{CPE}-1}$ , $P_{CPE} = 0.668$ , $R_{Ls} = 3.88 \, \Omega \, \text{cm}^2$ , $B_{Ls} = 0.0121 \, \text{s}^{\phi_{Ls}}$ , $\phi_{Ls} = 0.962$	98

To further corroborate the values of the specific surface area by impedance measurements, we also performed  $\text{N}_2$  adsorption experiments to evaluate the BET surface areas. Table 2 summarises the results of the BET specific surface areas of the CNT electrodes and of the CNT powder used to prepare the electrodes. To facilitate the comparison with the impedance results, all the specific surface area values are normalised by the mass of carbon (and, in addition, values normalised by the total mass of all the material are also reported). Table 2 shows that, as expected, the specific surface area decreases when the CNT powder is mixed with the binder to produce the electrode, due to the fact that the binder partially blocks some of the porosity of the CNT powder. More importantly, comparing the results of specific surface area values of the electrodes determined from impedance and BET analysis shows good agreement. Similarly, for the self-standing carbon electrodes made with acetylene black (Tables S1-2), both techniques also produce very similar results. Closer inspection shows that the BET specific surface area of the CNT electrodes is somewhat higher than the impedance specific surface area, which can be tentatively ascribed to the fact that some of the carbon microporosity is not fully filled with the electrolyte in the electrochemical cells, and thus, they do not contribute to the specific surface area determined by impedance. On the other hand, it should be noted that the  $\text{N}_2$  adsorption measurements of the electrodes were done by scratching the electrode coating from the current collector, which could produce some fragmentation and thus affect the surface area values. In summary, the impedance evaluation of surface areas is seen as the most reliable evaluation of the true electrode areas, but the fact that the BET surface areas are in good agreement further corroborates the reliability of the method of evaluation.

**Table 2.** Comparison of the specific surface areas (SAA) obtained by impedance and BET analysis of CNT and S/CNT electrodes and the CNT powder used for their preparation. Values are reported normalised by the mass of carbon ( $\text{m}^2 \, \text{g}_c^{-1}$ ), and for the BET measurements, also by the total mass of all materials ( $\text{m}^2 \, \text{g}_{tot}^{-1}$ ). Errors correspond to the confidence interval at 95% confidence level, obtained from at least three repeat experiments. The impedance SSA values are the average of all the measurements in Figure 5.

Material	BET SSA / $\text{m}^2 \, \text{g}_{tot}^{-1}$	BET SSA / $\text{m}^2 \, \text{g}_c^{-1}$	Impedance SSA / $\text{m}^2 \, \text{g}_c^{-1}$
CNT (powder)	$176 \pm 13$	$176 \pm 13$	N/A
CNT electrode	$112 \pm 14$	$127 \pm 16$	$89 \pm 8$

S/CNT electrode	$30 \pm 3$	$102 \pm 10$	$82 \pm 8$
-----------------	------------	--------------	------------

In conclusion, the electrochemical method of determination of the specific surface area of carbon electrodes by impedance is reproducible and reliable. In the next section, this technique is employed to understand the effect of the introduction of sulfur in the electrode formulation.

#### 4.2. Effect of sulfur on the specific surface area of carbon in carbon-sulfur composite electrodes

The impedance response of carbon-sulfur composite electrodes in symmetrical cells shows similar behaviour as that of carbon electrodes without sulfur. Figure S5 shows the impedance results obtained with electrodes made by mixing sulfur, CNT carbon additive and PEO+PVP binder (denoted here are 'S/CNT electrodes') in symmetrical cells (containing two nearly identical electrodes), showing that the results can be fitted to the same equivalent circuit as the cells containing the electrodes made with only CNT carbon additive and PEO+PVP binder (denoted here are 'CNT electrodes', Figure 4). This is because, under our experimental conditions, sulfur does not undergo any charge-transfer reaction producing polysulfides. The open circuit potential of sulfur electrodes in symmetrical cells is very high (ca. 3 V when referred to the  $\text{Li}^+/\text{Li}$  potential scale) [24, 59]. The impedance measurements are done by applying a small potential perturbation (10 mV of amplitude), and thus, the decrease in potential induced by the impedance measurements is not high enough to induce the reduction of sulfur to polysulfides. Effectively, sulfur remains electrochemically inactive in our measurements, and thus the impedance response is only due to the carbon present in the electrode.

Since carbon is the only electrochemically active component in the sulfur-carbon composite electrodes in the impedance measurements in symmetrical cells, by fitting the impedance data (see detail in the theory section), we obtain the specific surface area of carbon in the sulfur-carbon composite electrode. The results are included in Figure 5 as a function of the carbon loading in the electrode, together with the results of the carbon electrodes without sulfur. The difference between the results is smaller than the experimental reproducibility, showing that, for this particular electrode formulation, the addition of sulfur does not block the carbon surface area significantly. However, as will be shown below, the effect of sulfur on the specific surface area of conductive carbon in the electrode critically depends on the electrode formulation.

The effect of sulfur at blocking the surface area of the carbon contained in the electrode was then tested with a second electrode formulation, made with acetylene black and PTFE binder. As shown in Figure S3, the impedance response of the electrodes with sulfur is similar to that of the electrodes without sulfur (Figure S1), and the same equivalent circuit can be used for the fitting, from which the specific surface areas are evaluated (Tables S2-3). In this case, the addition of sulfur produces a noticeable decrease in the specific surface area of carbon, and increasing the sulfur content in the electrode produces a more significant effect on the decrease of the specific surface area. Similarly, the BET surface area also decreases with increasing sulfur content, although in this case the decrease is more marked. The more marked decrease of the BET surface area with the addition of sulfur is likely due to the fact that sulfur severely coats the acetylene black carbon particles, but when the specific surface area measurements are done inside the electrochemical cell via impedance measurements, some sulfur will dissolve in the electrolyte thus freeing a fraction of the carbon particles and



consequently, the impedance specific surface area is higher than the BET specific surface area for electrodes with high sulfur content.

In conclusion, impedance measurements can be used to reliably determine the specific surface area of carbon in carbon-sulfur composite electrodes relevant for Li-S battery applications. This approach is highly advantageous because the impedance measurements are fast and easy, and more importantly, they provide the relevant value of the specific surface area of carbon under the relevant conditions of operation of Li-S batteries, that is, in an electrochemical cell. In contrast, the BET measurements can produce an underestimation or overestimation of the specific surface area available for electrochemical reactions. Furthermore, previous work has shown that, when the electrode is exposed to vacuum for the BET measurements, redistribution of sulfur within the electrode can happen, thus potentially providing an unreliable measurement of the specific surface area [60].

In the following section, we demonstrate that impedance spectroscopy can also be employed to characterise the specific surface area of carbon in sulfur electrodes from direct measurements in Li-S cells.

#### **4.3. Direct evaluation of the specific surface area of carbon in carbon-sulfur composite electrodes in Li-S cells**

The analysis of the impedance response of Li-S cell is very challenging [40-54], due to the many different factors that contribute to the overall response. We have here developed a simple protocol by which the impedance response is drastically simplified and, hence, it can be used to directly evaluate the specific surface area of carbon in the carbon-sulfur composite electrode. Under these conditions, sulfur remains electrochemically inert, and the only response of the carbon-sulfur composite electrodes is due to the electrochemical double-layer charging of carbon, from which the specific surface area of carbon can be determined.

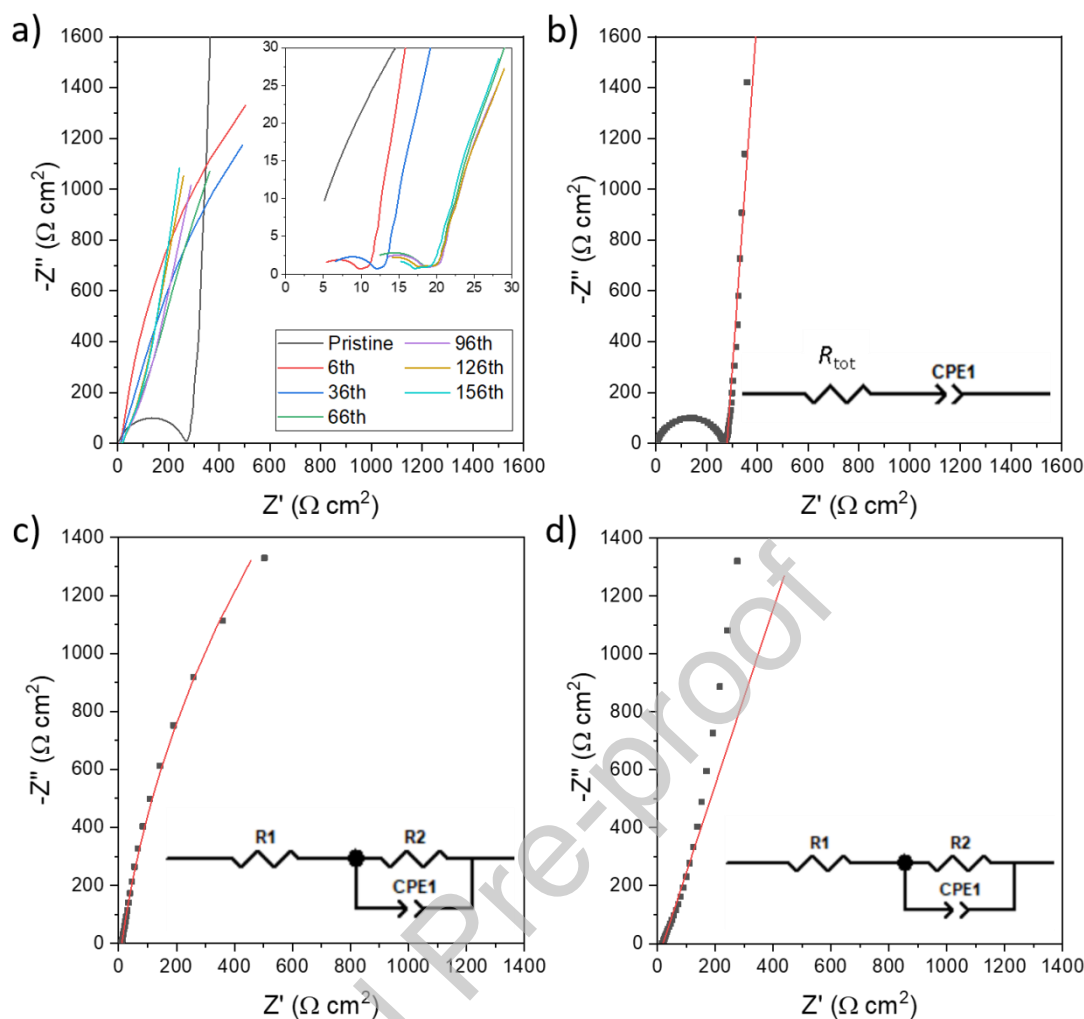
The conditions that enable the suppression of the electrochemical activity of sulfur are the following:

- 1) The impedance measurements are done in fully charged Li-S cells, polarised at high voltages (2.8 V during cell cycling and at the OCV for the pristine Li-S cells).
- 2) The fully charge state of Li-S cells is achieved by employing an optimised formulation of carbon-sulfur composite electrodes, made of a mixture of different carbon types and binders while maintaining a high sulfur content (65%wt), designed to produce high performance Li-S cells and suppression of the polysulfide shuttling [8, 55-57]. (Note that the polysulfide shuttling slowly discharges the Li-S cells and, thus, it prevents from reaching full charge [59, 61, 62]).
- 3) Use of a  $\text{LiNO}_3$ -containing electrolyte that induces the passivation of the lithium electrode, and further suppresses the polysulfide shuttling [63-65]. Specifically, we employ 1 M LiTFSI + 0.25 M  $\text{LiNO}_3$  in DOL/DME.

It is also worth mentioning that the Li-S cells were tested with an electrolyte to sulfur ratio of 6  $\mu\text{L mg}_\text{S}^{-1}$ , which was identified as optimal at providing high capacities and long cycle life under lean electrolyte conditions, based on a previous study by one of us, in which the same optimised S/C electrodes were tested in Li-S coin cells with electrolyte to sulfur ratios of 4-8  $\mu\text{L mg}_\text{S}^{-1}$  [56]. Indeed, Li-S coin cell studies rarely achieve good performance at this low electrolyte to sulfur ratio, while lower amounts of electrolyte can be used in pouch cells [4].

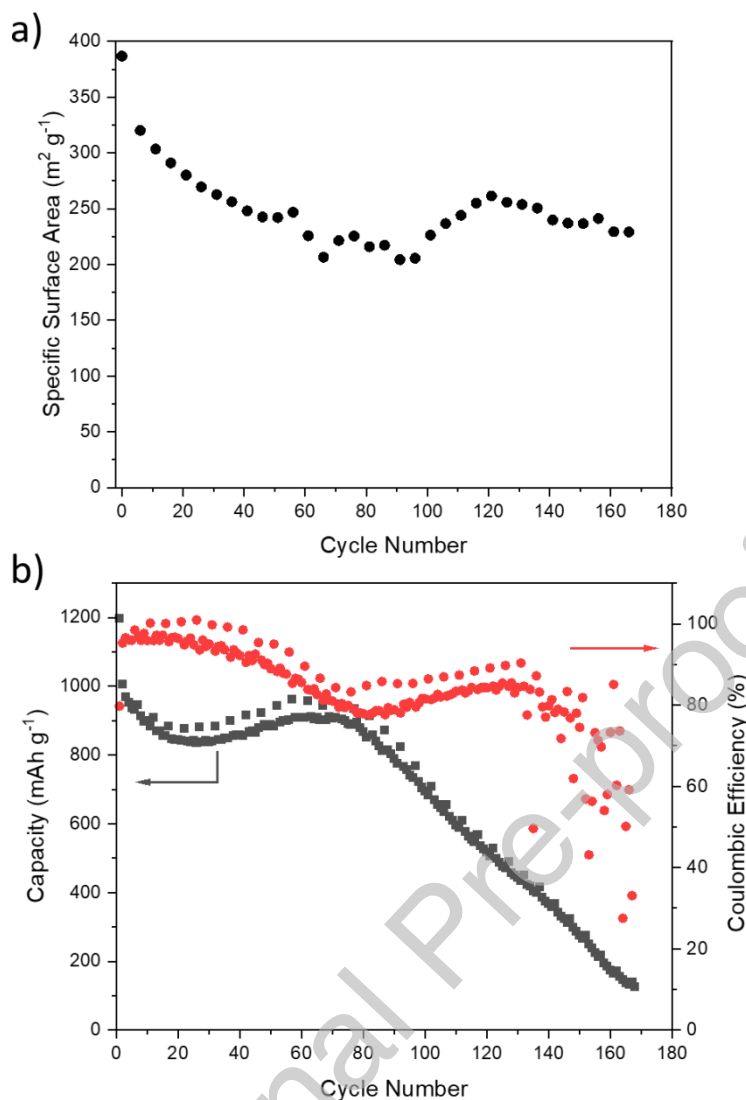
Figure 6 shows the impedance response of a Li-S cell measured under the above mentioned conditions. To minimise degradation of the cell at high voltages, the impedance measurements (at 2.8 V) were only taken every 5 cycles, and the other cycles were done with the standard upper voltage of 2.6 V. It is observed that the pristine cell shows a depressed semicircle of diameter of ca.  $200 \Omega \text{ cm}^2$  at high frequencies, which becomes much smaller in the cycled cells. This high-frequency semicircle can be attributed to the lithium electrode reactions, which become much faster after one cycle of lithium stripping and plating, due to the changes in the lithium electrode morphology (formation of mossy/dendritic lithium), as shown in previous work [66].

Based on the model experiments with carbon and carbon-sulfur composites (sections 4.1 and 4.2), we have shown that the impedance at low frequencies is dominated by the electrochemical response of carbon undergoing double-layer charging, which can be modelled with a constant phase element (CPE). Here we will show that all the rest of the elements in the Li-S cells can be modelled with a simple resistor. (Note that the simplification of using a simple resistor to model the behaviour of the separator and the lithium electrode at low frequencies is also supported by previous studies [66-70]). Figure 6b shows the fit of the impedance data to a combination of a resistor and a CPE in series, for the pristine Li-S cells. For the cycled cells, an additional resistor is included to improve the fit quality (Figure 6c,d), but essentially the same results of the evaluation of surface areas are obtained (less than 5% deviation) without that additional resistor. The additional resistor is used to model the very slow polysulfide shuttling process (or any other charge-transfer reaction such as, for example, electrolyte degradation at high voltages), and the very large value of resistance confirms that the process has been almost completely suppressed.



**Figure 6.** a) Impedance response of Li-S cells in the fully charged state: at OCV (ca. 2.9 V) for the pristine cell (i.e., before cycling) and 2.8 V for cycled cells, at the indicated cycle numbers. The cells contain an optimised S/C electrode formulation producing high performance (see details in the experimental section). b) Fit of the low frequency impedance of the pristine cell. c,d) Fit of the low frequency impedance of a cycled cell, for cycle number 6 and 156 in c) and d).

With the results of the Li-S cell impedance fitting, the specific surface area of carbon in the optimised S/C electrodes can be evaluated, as described in the Theory section, and the results are shown in Figure 7 as a function of the cycle number. The values of the parameters obtained from the fit are shown in Figure S6, and Figure S7-8 shows the results of a repeat experiment, displaying very good reproducibility.



**Figure 7.** a) Specific surface area (SSA) of carbon in the optimised S/C electrode formulation used in a Li-S cell (with carbon loading of  $1.79 \text{ mg}_c \text{ cm}^{-2}$ ), evaluated by fitting the impedance data in figure 6 to the equivalent circuits shown in the graph. b) Cycle performance of the same Li-S cell.

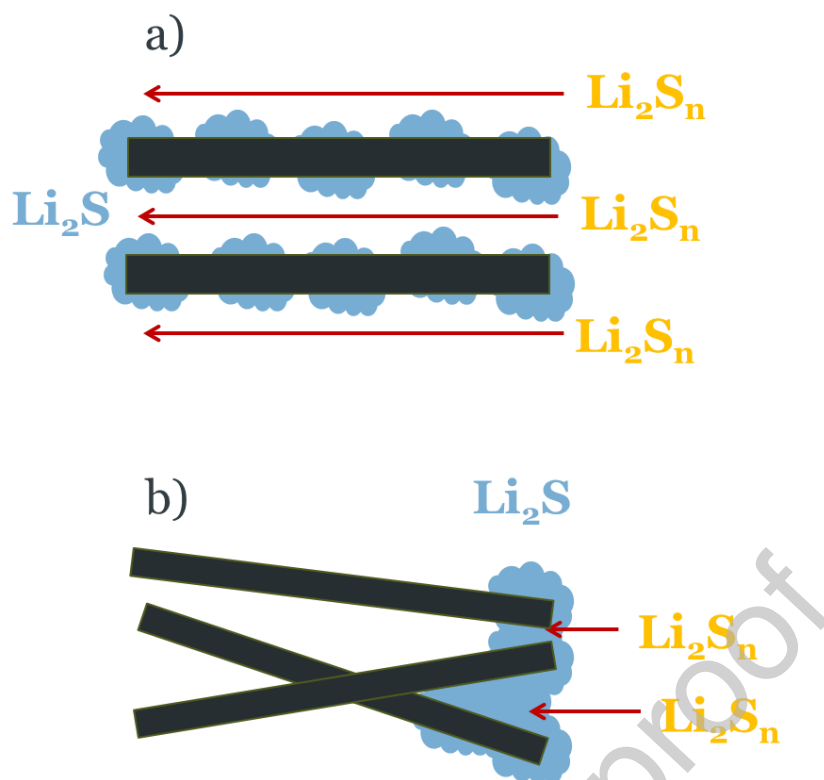
In order to validate the evaluation of the specific surface area of carbon from Li-S cells, additional experiments were done with the same optimised S/C electrodes used in the Li-S cell, but assembled in symmetric cells (by pairing two nearly identical S/C electrodes). Figure S9 shows the impedance response and the results of the evaluation of the specific surface area, which, on average, attains a value of  $274 \pm 19 \text{ m}^2 \text{ g}_c^{-1}$ . The values of the specific surface area of the pristine Li-S cells are found to be somewhat higher ( $387$  and  $359 \text{ m}^2 \text{ g}_c^{-1}$  for the cells in Figures 7 and S7, respectively). This difference can be tentatively ascribed to small alterations undergone by the electrodes when they were shipped from Uppsala, where they were produced, to Southampton, where they were tested in symmetrical cells, which were not present in the Li-S cell measurements, since they were done at Uppsala. The difference might also be caused by differences in cell design (Swagelok vs. coin cells for the symmetrical and Li-S cell measurements, respectively) or manual method of cell preparation (symmetrical and Li-S cell measurements were done by different researchers). However, after the first discharge and

charge cycle, the values of specific surface area of the Li-S cells (320 and 262 m<sup>2</sup> g<sub>c</sub><sup>-1</sup> for the cells in Figures 7 and S7, respectively) become closer to those measured in symmetrical cells, thus validating the method of analysis. As a side note, it is also worth noting that the impedance results of the optimised S/C electrodes in symmetrical cells (Figure S9) shows a much smaller magnitude of the high frequency semicircle than those of the S/CNT electrodes (Figure S5), indicating that a much better contact of the electrode coating with the aluminium foil substrate has been achieved with the optimised S/C electrodes, which can be attributed to the use of carbon coated aluminium foil substrates.

We will now discuss the effect of cycling on the values of the specific surface area of carbon in Li-S cells, shown in Figures 7 and S7. Some fluctuations in the specific surface area values are observed upon cycling, which can be attributed to the drastic morphology changes that the electrochemical reactions produce in the carbon-sulfur composite electrodes. However, the variations are not very marked. In contrast, the capacity of the cell significantly decreases with cycling beyond cycle number 80. This rapid capacity fade is due to the aggressive cycling conditions (long high voltage holds) required for the impedance measurements, since 'sister' Li-S cells last for hundreds of cycles under the standard cycling conditions (Figure S10). Apart from the faster capacity fade, the variation of the voltage profiles of the cells run with the impedance and standard protocols are very similar (Figure S11). On the other hand, the rapid capacity fade of the cells with impedance testing is advantageous here to facilitate the identification of the cause of cell death. After 170 cycles, the capacity is only 10% of the initial values, whereas the specific surface area is still around 70% of the initial value. Clearly, the capacity fade cannot be explained by only the decrease in surface area. The implications of these findings for guiding the rational development of Li-S batteries are discussed below.

## 5. Implications for further research

A good number of previous studies have suggested that passivation of the carbon matrix is a key factor determining the capacity and cycle life of Li-S batteries [13-21]. The reasoning behind the hypothesis that carbon passivation is a key factor stems from the fact that carbon is the only electrochemically active component of the sulfur electrodes and, thus, without carbon (or if carbon was fully passivated), the electrochemical reactions would not be able to proceed. In addition, it has also been experimentally shown that the choice of carbon makes an important effect on Li-S battery performance [3, 71-78], which again suggests that the electrochemical activity of carbon plays an important role in the continuation of Li-S battery reactions to reach high capacity and long cycle life. However, the results of the impedance analysis in Figure 7 clearly show that there is a significant amount of carbon with electrochemical activity (which, thus, contributes to the impedance measurements) for cells that exhibit very small capacity, demonstrating that other factors must be the cause of the capacity fading. These seemingly contradicting explanations can be brought together by taking into account the spatial heterogeneity of the sulfur electrode reactions, as illustrated in Figure 8.



**Figure 8.** Schematic illustration of the effect of the spatial heterogeneity of the sulfur electrode reactions in Li-S battery capacity: a) With fast transport of polysulfides (Li<sub>2</sub>S<sub>n</sub>) within the sulfur electrodes, the Li<sub>2</sub>S discharge product is deposited homogeneously in the whole electrode, thus delivering high capacity. b) With non-optimal sulfur electrode morphologies with narrow or tortuous paths for polysulfide (Li<sub>2</sub>S<sub>n</sub>) transport, the precipitation of Li<sub>2</sub>S discharge product blocks the paths and, hence, prevents further reactions, thus delivering low capacity. Li<sub>2</sub>S deposits are shown in blue, the black rectangles are carbon particles and lithium polysulfides (Li<sub>2</sub>S<sub>n</sub>) are shown in yellow.

The discharge of Li-S batteries involves the conversion of solid sulfur into soluble polysulfides and finally into solid Li<sub>2</sub>S. These ‘conversion’ processes involve a complex mixture of chemical and electrochemical reactions [7, 46, 79]. Fast chemical reactions between polysulfides enable the formation of Li<sub>2</sub>S suspended in solution, which, thus, can be formed in large quantities, producing high capacities; for example:



But the depletion of polysulfides due to slow mass transport would favour the direct electrochemical reduction of polysulfides, thus forming Li<sub>2</sub>S on the electrode surface:



Both reaction pathways (reactions 15 and 16) typically co-exist in Li-S batteries, and with non-tortuous sulfur electrodes allowing fast transport of electrolyte species (Figure 8a), nearly full conversion of sulfur to Li<sub>2</sub>S can be achieved. However, with tortuous sulfur electrodes, exhibiting narrow paths for electrolyte species transport (Figure 8b), the formation of Li<sub>2</sub>S is restricted to the areas of the electrode with fast access of electrolyte species. What is worse, in this case, the localised formation of Li<sub>2</sub>S blocks the channels for electrolyte species transport, and hence, only small amounts of Li<sub>2</sub>S can be formed in these batteries, and the capacity

delivered is small. Clearly, an extreme control of the electrode structure is required to achieve high Li-S battery performance.

The key role of fast polysulfide transport [6-8] and fast polysulfide chemical reactions [79-82] in Li-S batteries has been proposed before. It has also been shown that non-tortuous sulfur electrode formulations, deviating from the sulfur encapsulation approach, produce enhanced performance of Li-S batteries under lean electrolyte conditions (electrolyte to sulfur ratio of  $< 3 \mu\text{L mg}_\text{S}^{-1}$  in Li-S pouch cells) [83-85], and hence the challenge is to preserve such advantageous electrode morphologies during long cycling despite the drastic morphological changes induced by the electrochemical reactions [9-12]. The present impedance study provides a decisive proof that carbon passivation is not a performance limiting factor, for high performing Li-S batteries under lean electrolyte conditions. Consequently, the incorporation of high surface area carbons in the sulfur electrode formulation, for the purpose of preventing passivation, is not needed. The structural degradation of the electrode with cycling, producing slow electrolyte species mass transport, is proposed as a likely reason for the capacity fade. In addition, previous studies have shown that the reactivity of the lithium electrode with the electrolyte, and the drastic morphological changes undergone by the lithium electrode during cycling, are also very important issues affecting the cycle life of Li-S batteries made with a realistic cell design without a lithium anode excess [56, 65, 86-89] and, thus, these issues should receive closer attention.

## 6. Conclusions

This work demonstrates that impedance measurements of carbon and carbon-sulfur composites electrodes in symmetrical cells, and of fully charged lithium-sulfur cells, can be used to evaluate the electrochemically active specific surface area of the carbon conductive additive contained in the electrodes. The measurements are fast and simple and provide an accurate evaluation of the specific surface area of carbon under the relevant conditions of operation of lithium-sulfur batteries. Therefore, this method can be used to evaluate critical phenomena such as the passivation of carbon particles by sulfur or  $\text{Li}_2\text{S}$  deposition, as well as the loss of electrical contact between carbon particles, since these processes would decrease the specific surface area of carbon. These insights can be used to guide the development of formulations of sulfur electrodes as well as to identify the causes of capacity fade of Li-S batteries.

In this work, we show that for high-performing Li-S batteries with an optimised sulfur electrode formulation and lean electrolyte conditions, the decrease of capacity with cycling is not associated with a decrease in the carbon specific surface area of the sulfur electrode, thus demonstrating that the cause of the capacity fade is not due to a lack of carbon available to facilitate the electrochemical reactions. Consequently, improvements in performance should not be sought via the incorporation of higher surface area carbons. Instead, the focus should be shifted to address other issues such as mitigating adverse side-reactions at the lithium electrode and the development of sulfur electrodes with high structural stability to maintain fast polysulfide transport.

Credit author statement

**He Li:** Methodology, Investigation, Writing - original draft, Writing - review & editing. **John Lampkin:** Methodology, Investigation, Writing - review & editing. **Yu-Chuan Chien:**

Methodology, Investigation, Writing - review & editing. **Liam Furness:** Methodology, Investigation, Writing - review & editing. **Daniel Brandell:** Funding acquisition, Supervision, Writing - review & editing. **Matthew J. Lacey:** Funding acquisition, Supervision, Writing - review & editing. **Nuria Garcia-Araez:** Conceptualization, Funding acquisition, Supervision, Writing - review & editing

### Declaration of interests

The authors declare that they have no known competing financial interests or personal relationships that could have appeared to influence the work reported in this paper.

### Acknowledgments

Enlightening discussions with Prof. Andrzej Lasia are very gratefully acknowledged. Financial support from EPSRC through the Faraday Institution LiSTAR programme (EP/S003053/1, Grant FIRG014) and for an early career fellowship given to N.G.A (EP/N024303/1) is also gratefully acknowledged. D.B. and Y.-C.C. acknowledge support from the STandUP for Energy consortium. The data for this article are available from the University of Southampton at DOI: <https://doi.org/10.5258/SOTON/D2009>.

### References

- [1] M. Hagen, D. Hanselmann, K. Ahlbrecht, R. Maca, D. Gerber, J. Tubke, Lithium-Sulfur Cells: The Gap between the State-of-the-Art and the Requirements for High Energy Battery Cells, *Adv Energy Mater*, 5 (2015) 1401986.
- [2] D. Eroglu, K.R. Zavadil, K.G. Gallagher, Critical Link between Materials Chemistry and Cell-Level Design for High Energy Density and Low Cost Lithium-Sulfur Transportation Battery, *Journal of the Electrochemical Society*, 162 (2015) A982-A990.
- [3] S.-H. Chung, C.-H. Chang, A. Manthiram, Progress on the Critical Parameters for Lithium-Sulfur Batteries to be Practically Viable, *Advanced Functional Materials*, 28 (2018) 1801188.
- [4] S. Dörfler, H. Althues, P. Härtel, T. Abendroth, B. Schumm, S. Kaskel, Challenges and Key Parameters of Lithium-Sulfur Batteries on Pouch Cell Level, *Joule*, 4 (2020) 539-554.
- [5] G. Li, Z. Chen, J. Lu, Lithium-Sulfur Batteries for Commercial Applications, *Chem*, 4 (2018) 3-7.
- [6] T. Zhang, M. Marinescu, S. Walus, P. Kovacic, G.J. Offer, What Limits the Rate Capability of Li-S Batteries during Discharge: Charge Transfer or Mass Transfer?, *Journal of The Electrochemical Society*, 165 (2017) A6001-A6004.
- [7] S. Drvarič Talian, G. Kapun, J. Moškon, A. Vizintin, A. Randon-Vitanova, R. Dominko, M. Gaberšček, Which Process Limits the Operation of a Li-S System?, *Chemistry of Materials*, 31 (2019) 9012-9023.
- [8] Y.C. Chien, A.S. Menon, W.R. Brant, D. Brandell, M.J. Lacey, Simultaneous Monitoring of Crystalline Active Materials and Resistance Evolution in Lithium-Sulfur Batteries, *J Am Chem Soc*, 142 (2020) 1449-1456.
- [9] L. Zielke, C. Barchasz, S. Waluś, F. Alloin, J.C. Leprêtre, A. Spetl, V. Schmidt, A. Hilger, I. Manke, J. Banhart, R. Zengerle, S. Thiele, Degradation of Li/S Battery Electrodes On 3D Current Collectors Studied Using X-ray Phase Contrast Tomography, *Scientific Reports*, 5 (2015) 10921.



- [10] A. Yermukhambetova, C. Tan, S.R. Daemi, Z. Bakenov, J.A. Darr, D.J.L. Brett, P.R. Shearing, Exploring 3D microstructural evolution in Li-Sulfur battery electrodes using in-situ X-ray tomography, *Scientific Reports*, 6 (2016) 35291.
- [11] G. Tonin, G. Vaughan, R. Bouchet, F. Alloin, M. Di Michiel, L. Boutafa, J.-F. Colin, C. Barchasz, Multiscale characterization of a lithium/sulfur battery by coupling operando X-ray tomography and spatially-resolved diffraction, *Scientific Reports*, 7 (2017) 2755.
- [12] S.-H. Yu, X. Huang, K. Schwarz, R. Huang, T.A. Arias, J.D. Brock, H.D. Abruña, Direct visualization of sulfur cathodes: new insights into Li-S batteries via operando X-ray based methods, *Energy & Environmental Science*, 11 (2018) 202-210.
- [13] F.Y. Fan, W.C. Carter, Y.-M. Chiang, Mechanism and Kinetics of Li<sub>2</sub>S Precipitation in Lithium–Sulfur Batteries, *Advanced Materials*, 27 (2015) 5203-5209.
- [14] F.Y. Fan, Y.-M. Chiang, Electrodeposition Kinetics in Li-S Batteries: Effects of Low Electrolyte/Sulfur Ratios and Deposition Surface Composition, *Journal of The Electrochemical Society*, 164 (2017) A917-A922.
- [15] Z. Liu, P.P. Mukherjee, Mesoscale Elucidation of Surface Passivation in the Li-Sulfur Battery Cathode, *ACS Appl Mater Interfaces*, 9 (2017) 5263-5271.
- [16] P. Andrei, C. Shen, J.P. Zheng, Theoretical and experimental analysis of precipitation and solubility effects in lithium-sulfur batteries, *Electrochimica Acta*, 284 (2018) 469-484.
- [17] H. Pan, K.S. Han, M.H. Engelhard, R. Cao, J. Chen, J.-G. Zhang, K.T. Mueller, Y. Shao, J. Liu, Addressing Passivation in Lithium–Sulfur Battery Under Lean Electrolyte Condition, *Advanced Functional Materials*, 28 (2018) 1707234.
- [18] Z. Li, Y. Zhou, Y. Wang, Y.-C. Lu, Solvent-Mediated Li<sub>2</sub>S Electrodeposition: A Critical Manipulator in Lithium–Sulfur Batteries, *Adv Energy Mater*, 9 (2019) 1802207.
- [19] C. Shen, P. Andrei, J.P. Zheng, Unraveling the Li<sub>2</sub>S Deposition Process on a Polished Graphite Cathode for Enhancing Discharge Capacity of Lithium–Sulfur Batteries, *ACS Applied Energy Materials*, 2 (2019) 3860-3868.
- [20] H. Chu, H. Noh, Y.J. Kim, S. Yuk, J.H. Lee, J. Lee, H. Kwack, Y. Kim, D.K. Yang, H.T. Kim, Achieving three-dimensional lithium sulfide growth in lithium-sulfur batteries using high-donor-number anions, *Nat Commun*, 10 (2019) 188.
- [21] L. Kong, J.-X. Chen, H.-J. Peng, J.-Q. Huang, W. Zhu, Q. Jin, B.-Q. Li, X.-T. Zhang, Q. Zhang, Current-density dependence of Li<sub>2</sub>S/Li<sub>2</sub>S<sub>2</sub> growth in lithium–sulfur batteries, *Energy & Environmental Science*, 12 (2019) 2976-2982.
- [22] P. Delahay, C.W. Tobias, *Advances in Electrochemistry and Electrochemical Engineering: Electrochemistry. Volume 6*, Interscience Publishers, 1967.
- [23] A. Lasia, *Electrochemical Impedance Spectroscopy and its Applications*, Springer New York, 2014.
- [24] R. Raccichini, L. Furness, J.W. Dibden, J.R. Owen, N. Garcia-Araez, Impedance Characterization of the Transport Properties of Electrolytes Contained within Porous Electrodes and Separators Useful for Li-S Batteries, *Journal of the Electrochemical Society*, 165 (2018) A2741-A2749.
- [25] J. Lampkin, H. Li, L. Furness, R. Raccichini, N. Garcia-Araez, A Critical Evaluation of the Effect of Electrode Thickness and Side Reactions on Electrolytes for Aluminum-Sulfur Batteries, *ChemSusChem*, 13 (2020) 3514-3523.
- [26] M. Adamič, S.D. Talian, A.R. Sinigoj, I. Humar, J. Moškon, M. Gaberšček, A Transmission Line Model of Electrochemical Cell's Impedance: Case Study on a Li-S System, *Journal of The Electrochemical Society*, 166 (2018) A5045-A5053.
- [27] N. Ogihara, S. Kawauchi, C. Okuda, Y. Itou, Y. Takeuchi, Y. Ukyo, Theoretical and Experimental Analysis of Porous Electrodes for Lithium-Ion Batteries by Electrochemical Impedance Spectroscopy Using a Symmetric Cell, *Journal of The Electrochemical Society*, 159 (2012) A1034-A1039.

- [28] J. Landesfeind, J. Hattendorff, A. Ehrl, W.A. Wall, H.A. Gasteiger, Tortuosity Determination of Battery Electrodes and Separators by Impedance Spectroscopy, *Journal of the Electrochemical Society*, 163 (2016) A1373-A1387.
- [29] J. Landesfeind, A. Eldiven, H.A. Gasteiger, Influence of the Binder on Lithium Ion Battery Electrode Tortuosity and Performance, *Journal of The Electrochemical Society*, 165 (2018) A1122-A1128.
- [30] J. Landesfeind, M. Ebner, A. Eldiven, V. Wood, H.A. Gasteiger, Tortuosity of Battery Electrodes: Validation of Impedance-Derived Values and Critical Comparison with 3D Tomography, *Journal of The Electrochemical Society*, 165 (2018) A469-A476.
- [31] S. Oswald, D. Pritzl, M. Wetjen, H.A. Gasteiger, Novel Method for Monitoring the Electrochemical Capacitance by In Situ Impedance Spectroscopy as Indicator for Particle Cracking of Nickel-Rich NCMs: Part I. Theory and Validation, *Journal of The Electrochemical Society*, 167 (2020) 100511.
- [32] V. Charbonneau, A. Lasia, G. Brisard, Impedance studies of Li<sup>+</sup> diffusion in nickel manganese cobalt oxide (NMC) during charge/discharge cycles, *Journal of Electroanalytical Chemistry*, 875 (2020) 113944.
- [33] G.J. Brug, A.L.G. van den Eeden, M. Sluyters-Rehbach, J.H. Sluyters, The analysis of electrode impedances complicated by the presence of a constant phase element, *Journal of Electroanalytical Chemistry and Interfacial Electrochemistry*, 176 (1984) 275-295.
- [34] B. Hirschorn, M.E. Orazem, B. Tribollet, V. Vivier, I. Frateur, M. Musiani, Determination of effective capacitance and film thickness from constant-phase-element parameters, *Electrochimica Acta*, 55 (2010) 6218-6227.
- [35] A. Lasia, Impedance of porous electrodes, *Journal of Electroanalytical Chemistry*, 397 (1995) 27-33.
- [36] R. Jurczakowski, C. Hitz, A. Lasia, Impedance of porous Au based electrodes, *Journal of Electroanalytical Chemistry*, 572 (2004) 355-366.
- [37] J. Huang, B.G. Sumpter, V. Meunier, Theoretical Model for Nanoporous Carbon Supercapacitors, *Angewandte Chemie International Edition*, 47 (2008) 520-524.
- [38] M. Gaberscek, J. Moskon, B. Erjavec, R. Dominko, J. Jamnik, The importance of interphase contacts in Li ion electrodes: The meaning of the high-frequency impedance arc, *Electrochem Solid St*, 11 (2008) A170-A174.
- [39] G. Carbonari, V. Müller, R.-G. Scurtu, M. Memm, A. Hoffmann, M. Wohlfahrt-Mehrens, Communication—Edge Quality Contribution on the Electrical Impedance of Lithium-Ion Batteries Electrodes, *Journal of The Electrochemical Society*, 167 (2020) 080504.
- [40] V.S. Kolosnitsyn, E.V. Kuzmina, E.V. Karaseva, S.E. Mochalov, A study of the electrochemical processes in lithium–sulphur cells by impedance spectroscopy, *Journal of Power Sources*, 196 (2011) 1478-1482.
- [41] Z. Deng, Z. Zhang, Y. Lai, J. Liu, J. Li, Y. Liu, Electrochemical Impedance Spectroscopy Study of a Lithium/Sulfur Battery: Modeling and Analysis of Capacity Fading, *Journal of The Electrochemical Society*, 160 (2013) A553-A558.
- [42] N.A. Cañas, K. Hirose, B. Pascucci, N. Wagner, K.A. Friedrich, R. Hiesgen, Investigations of lithium–sulfur batteries using electrochemical impedance spectroscopy, *Electrochimica Acta*, 97 (2013) 42-51.
- [43] D.N. Fronczek, W.G. Bessler, Insight into lithium–sulfur batteries: Elementary kinetic modeling and impedance simulation, *Journal of Power Sources*, 244 (2013) 183-188.
- [44] S. Risse, N.A. Cañas, N. Wagner, E. Hürk, M. Ballauff, K.A. Friedrich, Correlation of capacity fading processes and electrochemical impedance spectra in lithium/sulfur cells, *Journal of Power Sources*, 323 (2016) 107-114.
- [45] A. Ganesan, A. Varzi, S. Passerini, M.M. Shaijumon, Graphene derived carbon confined sulfur cathodes for lithium-sulfur batteries: Electrochemical impedance studies, *Electrochimica Acta*, 214 (2016) 129-138.

- [46] S. Drvaric Talian, J. Moskon, R. Dominko, M. Gaberscek, Reactivity and Diffusivity of Li Polysulfides: A Fundamental Study Using Impedance Spectroscopy, *ACS Appl Mater Interfaces*, 9 (2017) 29760-29770.
- [47] J. Conder, C. Villevieille, S. Trabesinger, P. Novák, L. Gubler, R. Bouchet, Electrochemical impedance spectroscopy of a Li-S battery: Part 1. Influence of the electrode and electrolyte compositions on the impedance of symmetric cells, *Electrochimica Acta*, 244 (2017) 61-68.
- [48] J. Conder, C. Villevieille, S. Trabesinger, P. Novák, L. Gubler, R. Bouchet, Electrochemical impedance spectroscopy of a Li-S battery: Part 2. Influence of separator chemistry on the lithium electrode/electrolyte interface, *Electrochimica Acta*, 255 (2017) 379-390.
- [49] C.-F. Chen, A. Mistry, P.P. Mukherjee, Probing Impedance and Microstructure Evolution in Lithium-Sulfur Battery Electrodes, *The Journal of Physical Chemistry C*, 121 (2017) 21206-21216.
- [50] S. Drvarič Talian, J. Moškon, R. Dominko, M. Gaberšček, Impedance response of porous carbon cathodes in polysulfide redox system, *Electrochimica Acta*, 302 (2019) 169-179.
- [51] J. Fang, W. Shen, S.H.S. Cheng, S. Ghashghaie, H.K. Shahzad, C.Y. Chung, Four-electrode symmetric setup for electrochemical impedance spectroscopy study of Lithium-Sulfur batteries, *Journal of Power Sources*, 441 (2019) 227202.
- [52] X. Qiu, Q. Hua, L. Zheng, Z. Dai, Study of the discharge/charge process of lithium-sulfur batteries by electrochemical impedance spectroscopy, *RSC Advances*, 10 (2020) 5283-5293.
- [53] S. Waluś, C. Barchasz, R. Bouchet, F. Alloin, Electrochemical impedance spectroscopy study of lithium-sulfur batteries: Useful technique to reveal the Li/S electrochemical mechanism, *Electrochimica Acta*, 359 (2020) 136944.
- [54] A. Kilic, D. Eroglu, Characterization of the Effect of Cell Design on Li-S Battery Resistance Using Electrochemical Impedance Spectroscopy, *ChemElectroChem*, 8 (2021) 963-971.
- [55] M.J. Lacey, V. Osterlund, A. Bergfelt, F. Jeschull, T. Bowden, D. Brandell, A Robust, Water-Based, Functional Binder Framework for High-Energy Lithium-Sulfur Batteries, *ChemSusChem*, 10 (2017) 2758-2766.
- [56] M.J. Lacey, Influence of the Electrolyte on the Internal Resistance of Lithium-Sulfur Batteries Studied with an Intermittent Current Interruption Method, *ChemElectroChem*, 4 (2017) 1997-2004.
- [57] Y.-C. Chien, R. Pan, M.-T. Lee, L. Nyholm, D. Brandell, M.J. Lacey, Cellulose Separators With Integrated Carbon Nanotube Interlayers for Lithium-Sulfur Batteries: An Investigation into the Complex Interplay between Cell Components, *Journal of The Electrochemical Society*, 166 (2019) A3235-A3241.
- [58] M. Gaberscek, J. Moskon, B. Erjavec, R. Dominko, J. Jamnik, The Importance of Interphase Contacts in Li Ion Electrodes: The Meaning of the High-Frequency Impedance Arc, *Electrochemical and Solid-State Letters*, 11 (2008) A170.
- [59] S.M. Al-Mahmoud, J.W. Diben, J.R. Owen, G. Denuault, N. Garcia-Araez, A simple, experiment-based model of the initial self-discharge of lithium-sulphur batteries, *Journal of Power Sources*, 306 (2016) 323-328.
- [60] C. Reiß, K. Peppler, J. Janek, P. Adelhelm, Pitfalls in the characterization of sulfur/carbon nanocomposite materials for lithium-sulfur batteries, *Carbon*, 79 (2014) 245-255.
- [61] Y.V. Mikhaylik, J.R. Akridge, Polysulfide Shuttle Study in the Li/S Battery System, *Journal of The Electrochemical Society*, 151 (2004) A1969.
- [62] M.J. Lacey, A. Yalamanchili, J. Maibach, C. Tengstedt, K. Edström, D. Brandell, The Li-S battery: an investigation of redox shuttle and self-discharge behaviour with LiNO<sub>3</sub>-containing electrolytes, *RSC Advances*, 6 (2016) 3632-3641.
- [63] Y.V. Mikhaylik, Electrolytes for lithium sulfur cells, Sion Power Corp, US, 2008.
- [64] D. Aurbach, E. Pollak, R. Elazari, G. Salitra, C.S. Kelley, J. Affinito, On the Surface Chemical Aspects of Very High Energy Density, Rechargeable Li-Sulfur Batteries, *Journal of The Electrochemical Society*, 156 (2009) A694.

- [65] Y.V. Mikhaylik, I. Kovalev, R. Schock, K. Kumaresan, J. Xu, J. Affinito, High Energy Rechargeable Li-S Cells for EV Application: Status, Remaining Problems and Solutions, *ECS Transactions*, 25 (2019) 23-34.
- [66] S. Drvarič Talian, J. Bobnar, A.R. Sinigoj, I. Humar, M. Gaberšček, Transmission Line Model for Description of the Impedance Response of Li Electrodes with Dendritic Growth, *The Journal of Physical Chemistry C*, 123 (2019) 27997-28007.
- [67] J.G. Thevenin, R.H. Muller, Impedance of Lithium Electrodes in a Propylene Carbonate Electrolyte, *Journal of The Electrochemical Society*, 134 (1987) 273-280.
- [68] D. Aurbach, A. Zaban, Impedance spectroscopy of lithium electrodes: Part 1. General behavior in propylene carbonate solutions and the correlation to surface chemistry and cycling efficiency, *Journal of Electroanalytical Chemistry*, 348 (1993) 155-179.
- [69] M. Morita, S. Aoki, Y. Matsuda, ac impedance behaviour of lithium electrode in organic electrolyte solutions containing additives, *Electrochimica Acta*, 37 (1992) 119-123.
- [70] N. Takami, T. Ohsaki, K. Inada, The Impedance of Lithium Electrodes in LiPF<sub>6</sub> - Based Electrolytes, *Journal of The Electrochemical Society*, 139 (1992) 1849-1854.
- [71] X. Ji, L.F. Nazar, Advances in Li-S batteries, *Journal of Materials Chemistry*, 20 (2010) 9821-9826.
- [72] Y. Yang, G. Zheng, Y. Cui, Nanostructured sulfur cathodes, *Chemical Society Reviews*, 42 (2013) 3018-3032.
- [73] A. Manthiram, Y. Fu, S.H. Chung, C. Zu, Y.S. Su, Rechargeable lithium-sulfur batteries, *Chem Rev*, 114 (2014) 11751-11787.
- [74] S. Urbonaite, T. Poux, P. Novák, Progress Towards Commercially Viable Li-S Battery Cells, *Adv Energy Mater*, 5 (2015) 1500118.
- [75] R. Sahore, B.D.A. Levin, M. Pan, D.A. Muller, F.J. DiSalvo, E.P. Giannelis, Design Principles for Optimum Performance of Porous Carbons in Lithium-Sulfur Batteries, *Adv Energy Mater*, 6 (2016) 1600134.
- [76] L. Borchardt, M. Oschatz, S. Kaskel, Carbon Materials for Lithium Sulfur Batteries—Ten Critical Questions, *Chemistry – A European Journal*, 22 (2016) 7324-7351.
- [77] M. Zhao, B.Q. Li, H.J. Peng, H. Yuan, J.Y. Wei, J.Q. Huang, Lithium-Sulfur Batteries under Lean Electrolyte Conditions: Challenges and Opportunities, *Angew Chem Int Ed Engl*, 59 (2020) 12636-12652.
- [78] L. Huang, J. Li, B. Liu, Y. Li, S. Shen, S. Deng, C. Lu, W. Zhang, Y. Xia, G. Pan, X. Wang, Q. Xiong, X. Xia, J. Tu, Electrode Design for Lithium-Sulfur Batteries: Problems and Solutions, *Advanced Functional Materials*, 30 (2020) 1910375.
- [79] Y.-C. Lu, Q. He, H.A. Gasteiger, Probing the Lithium-Sulfur Redox Reactions: A Rotating-Ring Disk Electrode Study, *The Journal of Physical Chemistry C*, 118 (2014) 5733-5741.
- [80] A. Berger, A.T.S. Freiberg, A. Siebel, R. Thomas, M.U.M. Patel, M. Tromp, H.A. Gasteiger, Y. Gorlin, The Importance of Chemical Reactions in the Charging Process of Lithium-Sulfur Batteries, *Journal of The Electrochemical Society*, 165 (2018) A1288-A1296.
- [81] Y. Gorlin, A. Siebel, M. Piana, T. Huthwelker, H. Jha, G. Monsch, F. Kraus, H.A. Gasteiger, M. Tromp, Operando Characterization of Intermediates Produced in a Lithium-Sulfur Battery, *Journal of The Electrochemical Society*, 162 (2015) A1146-A1155.
- [82] Y. Gorlin, M.U.M. Patel, A. Freiberg, Q. He, M. Piana, M. Tromp, H.A. Gasteiger, Understanding the Charging Mechanism of Lithium-Sulfur Batteries Using Spatially Resolved Operando X-Ray Absorption Spectroscopy, *Journal of The Electrochemical Society*, 163 (2016) A930-A939.
- [83] M. Agostini, J.-Y. Hwang, H.M. Kim, P. Bruni, S. Brutti, F. Croce, A. Matic, Y.-K. Sun, Minimizing the Electrolyte Volume in Li-S Batteries: A Step Forward to High Gravimetric Energy Density, *Adv Energy Mater*, 8 (2018) 1801560.

- [84] Y. Xie, G. Pan, Q. Jin, X. Qi, T. Wang, W. Li, H. Xu, Y. Zheng, S. Li, L. Qie, Y. Huang, J. Li, Semi-Flooded Sulfur Cathode with Ultralean Absorbed Electrolyte in Li-S Battery, *Advanced Science*, 7 (2020) 1903168.
- [85] L. Shi, S.-M. Bak, Z. Shadike, C. Wang, C. Niu, P. Northrup, H. Lee, A.Y. Baranovskiy, C.S. Anderson, J. Qin, S. Feng, X. Ren, D. Liu, X.-Q. Yang, F. Gao, D. Lu, J. Xiao, J. Liu, Reaction heterogeneity in practical high-energy lithium-sulfur pouch cells, *Energy & Environmental Science*, 13 (2020) 3620-3632.
- [86] M.J. Lacey, K. Edström, D. Brandell, Visualising the problems with balancing lithium-sulfur batteries by “mapping” internal resistance, *Chemical Communications*, 51 (2015) 16502-16505.
- [87] M.-T. Lee, H. Liu, D. Brandell, The Surface Chemistry of Thin Lithium Metal Electrodes in Lithium-Sulfur Cells, *Batteries Supercaps*, 3 (2020) 1370-1376.
- [88] X.-B. Cheng, C. Yan, J.-Q. Huang, P. Li, L. Zhu, L. Zhao, Y. Zhang, W. Zhu, S.-T. Yang, Q. Zhang, The gap between long lifespan Li-S coin and pouch cells: The importance of lithium metal anode protection, *Energy Storage Materials*, 6 (2017) 18-25.
- [89] Y.C. Chien, D. Brandell, M.J. Lacey, Towards reliable three-electrode cells for lithium-sulfur batteries, *ChemRxiv*, (2021) 10.33774/chemrxiv-32021-gznvz.